Pattern Formation in Polymerizing Actin Flocks: Spirals, Spots, and Waves without Nonlinear Chemistry

T. Le Goff,* B. Liebchen,† and D. Marenduzzo
SUPA, School of Physics and Astronomy, University of Edinburgh, Peter Guthrie Tait Road, Edinburgh, EH9 3FD, United Kingdom
(Received 5 August 2016; revised manuscript received 14 October 2016; published 30 November 2016)

We propose a model solely based on actin treadmilling and polymerization which describes many characteristic states of actin-wave formation: spots, spirals, and traveling waves. In our model, as in experiments on cells recovering motility following actin depolymerization, we choose an isotropic low-density initial condition; polymerization of actin filaments then raises the density towards the Onsager threshold where they align. We show that this alignment, in turn, destabilizes the isotropic phase and generically induces transient actin spots or spirals as part of the dynamical pathway towards a polarized phase which can either be uniform or consist of a series of actin-wave trains (flocks). Our results uncover a universal route to actin-wave formation in the absence of any system-specific nonlinear biochemistry, and it may help to understand the mechanism underlying the observation of actin spots and waves *in vivo*. They also suggest a minimal setup to design similar patterns *in vitro*.

DOI: 10.1103/PhysRevLett.117.238002

Actin networks are highly dynamic subcellular structures which constitute a key component of the cytoskeleton of eukaryotic cells [1]. These networks are cross-linked gels made up from actin filaments, semiflexible fibers with persistence and contour lengths both in the 1–10 μm range. Actin filaments are active polymers which function far from thermodynamic equilibrium, as they constantly turn over their components, actin monomers, through polymerization and depolymerization: the dynamics of these networks also provide the microscopic basis of cell motility [1–3].

Actin filaments and networks self-organize into a variety of mesmerizing patterns [4–6]. *In vitro*, experiments have reported the formation of lanes, waves, and spirals in systems where actin fibers walk on a carpet of immobilized molecular motors [4]. *In vivo*, the actin network of a cell is normally localized within a micrometer-wide cortex trailing just behind the advancing membrane of a crawling cell [2]. However, under particular conditions, actin fibers reorganize within the cell and create different patterns, such as traveling or scroll waves bound to the two-dimensional cell membrane [5–9].

In some cases, the mechanism through which actin waves arise is relatively well understood and depends on a network of biochemical regulatory reactions involving actin-associated proteins [10], which can be effectively modeled as an activator-inhibitor dynamical system. Such models, based on nonlinear biochemistry, successfully explain cases where actin waves are associated with the activation of the SCAR-WAVE complex [11], and they are linked to chemotaxis [12]. However, there are other examples where waves depend on only a small number of components. Most relevant to our work are the waves observed in *Dictyostelium* cells recovering from treatment with latrunculin, which causes mass depolymerization of actin fibers [5,6]. When latrunculin is taken away, actin fibers repolymerize from monomers in the cytosol, and after this cells recover motility: They do so by undergoing a surprisingly complex pattern formation cascade. First, actin assembles into transient spots, which then evolve into waves; spiral patterns are also observed in some cases. A set of experiments knocking out several actin-associated proteins clarified that the dynamics leading to waves is not dependent, among others, on the SCAR-WAVE complex or on contractile myosin motors [6].

The waves observed in Ref. [5] have to date been addressed by a number of models in the literature [13–17]. All these lead to wave formation, and all include some nonlinear dynamics, such as the Fitz-Nagumo model [13], or other activator-inhibitor models [14]. This choice is motivated by the observation that some actin-associated proteins *are* found in waves—most notably, coronin, which localizes at the rear of a wave, and myosin I, which lies at the front [6]. While these are all perfectly plausible models, they rely either on the existence of a delay or on (cubic) nonlinear reaction terms which are generally quite system-specific.

Here we suggest an alternative model for wave formation, which does not require *any* nonlinear biochemistry and solely depends on three simple and generic ingredients: actin polymerization, steric repulsion between actin fibers, and treadmilling (i.e., the effective motion of actin fibers which grow at one end and shrink at the other one [1,2]). Since all three ingredients occur in a wide class of systems featuring actin waves, our findings suggest that spots and waves could hinge on a universal mechanism and do not, as the current literature suggests, require system-specific nonlinear chemistry. This key finding should be relevant

for the current understanding of waves in *Dictyostelium in vivo*; it also suggests how to set up experiments *in vitro* to generate similar patterns.

In our model, actin filaments "flock" [18]: they align when dense enough, due to excluded volume interactions (like rigid rods in the Onsager theory [19]), and they move due to treadmilling, leading to actin waves. At the low initial fiber densities typical of the early stages of experiments in *Dictyostelium*, however, alignment interactions are ineffective. As a preliminary step to wave formation, polymerization increases the fiber density. Here, we unveil that spot formation, which is frequently observed in experiments prior to waves [5], does not require complex reaction-based instabilities but occurs *generically* as part of the dynamical pathway from the isotropic to the flocking phase. Polymerization shapes the morphology of the emerging waves, and allows us to control their length scale.

To specify our qualitative arguments, we now propose a two-dimensional dynamical model to study pattern formation in a system of polymerizing actin fibers. This geometry was also chosen in previous studies [13] as it matches that of the experiments in Ref. [6], where patterns form anywhere on the 2D cell membrane and reach at most $\sim 1\ \mu$m in height. We follow both the density of actin in filaments (F-actin), ρ, and the average filament polarization (i.e., the sum of orientation unit vectors per unit volume) $\mathbf{P}$. The equations of motion defining our model are

$$\partial_t \rho = -v_0 \boldsymbol{\nabla} \cdot (\rho \mathbf{P}) + D_\rho \boldsymbol{\nabla}^2 \rho + \alpha \rho \left(1 - \frac{\rho}{\rho_0}\right), \quad (1)$$

$$\partial_t \mathbf{P} = \gamma \left(\frac{\rho}{\rho_c} - 1\right) \mathbf{P} + K \boldsymbol{\nabla}^2 \mathbf{P} - \gamma_2 P^2 \mathbf{P}. \quad (2)$$

Here D_ρ is the diffusion coefficient of F-actin and K is an effective elastic constant, while v_0 and α denote the treadmilling speed and the polymerization rate, respectively. The reaction term $\alpha\rho$ describes both the growth of existing F-actin fibers and Arp2/3-dependent nucleation of new fibers; this term is proportional to ρ as both phenomena require preexisting F-actin fibers [20]. The saturation term $-\alpha\rho^2/\rho_0$ arises as crowding slows down polymerization. Furthermore, γ measures how fast F-actin filaments change their direction, and the term in γ_2 ensures saturation of the polarization, whereas ρ_c and ρ_0 indicate, respectively, the critical density above which orientational order sets in and the target polymerization density (i.e., the density of F-actin which would be reached due to polymerization in a well-stirred system in the absence of spatial effects). For $\alpha = 0$, Eqs. (1) and (2) are related to the models of Refs. [21–24], although even in that limit our emphasis here is on the dynamical pathway the system follows rather than on steady state behavior. Conversely, for $v_0 = 0$ Eq. (1) reduces to the Fisher-Kolmogorov equation [25].

It is useful to recast Eqs. (1) and (2) in terms of dimensionless variables, as follows:

$$\partial_t \rho = -\boldsymbol{\nabla} \cdot (\rho \mathbf{P}) + \boldsymbol{\nabla}^2 \rho + \rho(1 - \rho), \quad (3)$$

$$\partial_t \mathbf{P} = \Gamma(r\rho - 1)\mathbf{P} + \mathcal{D}\boldsymbol{\nabla}^2 \mathbf{P} - \Gamma_2 P^2 \mathbf{P}, \quad (4)$$

where we have defined $\Gamma = \gamma/\alpha$, $r = \rho_0/\rho_c$, $\mathcal{D} = K/D_\rho$, and $\Gamma_2 = \gamma_2 D_\rho / v_0^2$ and redefined $t \to \alpha t$, $x \to (\alpha/D_\rho)^{1/2} x$, $\rho \to \rho/\rho_0$, and $\mathbf{P} \to (v_0/\sqrt{D_\rho \alpha})\mathbf{P}$. Equations (3) and (4) clarify that the dynamics of our model depends on four dimensionless parameters—while we have varied all of these, Γ, which is the ratio between alignment and the polymerization rate, is our key control parameter (provided that $r > 1$). Thus, we vary Γ in the following while keeping other parameters fixed (see the caption of Fig. 1). It is useful to estimate the experimentally relevant orders of magnitude of parameter values. *In vivo* or in the lab, actin may polymerize at a rate $\alpha \sim 1$–$100\ \mathrm{s}^{-1}$ [2,26], while γ may be estimated as the rotational diffusion D_r of an intracellular F-actin filament of typical geometry $\sim 1\ \mu\mathrm{m} \times \sim 5$ nm, which is $\sim 10\ \mathrm{s}^{-1}$ [26]. For this geometry, the Onsager threshold of actin fibers is $\sim 0.5\%$ in volume fraction—the inverse of their aspect ratio—whereas the F-actin density in a cell is up to $\sim 10\ \mathrm{g}/l$ [27] or $\sim 1\%$ in volume fraction. Consequently, an experimentally relevant range of parameters is $\Gamma \sim 0.1$–10 and $r > 1$. Following the procedure in Ref. [28], we can write $\Gamma_2 = \gamma^2 D_\rho / (2 D_r v_0^2)$. For typical molecular diffusion coefficients of $D_\rho \sim 10^{-12}$–$10^{-11}\ \mathrm{m}^2/\mathrm{s}$, this yields $\Gamma_2 \sim 0.01$–1, justifying our choice of $\Gamma_2 = 0.075$ in Figs. 1 and 3.

We have solved Eqs. (3) and (4) for different values of Γ on a square lattice of size $L_x \times L_y$ using finite difference methods, periodic boundary conditions, and a uniform

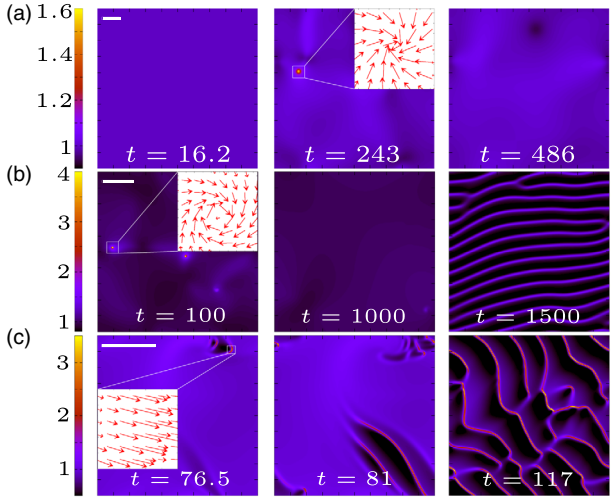

FIG. 1. Representative snapshots for actin pattern formation as described in the main text. (a) $\Gamma = 1$; (b) $\Gamma = 4.3$; (c) $\Gamma = 10$. Other parameters: $r = 1.1$, $\mathcal{D} = 5$, and $\Gamma_2 = 0.075$. The scale bar is 50.

initial state $\{\rho, \mathbf{p}\} = (0, \mathbf{0})$ plus some small fluctuations. For identical polymerization and alignment rate ($\Gamma = 1$), we initially observe a uniform density growth followed, after a certain lag time, by the formation of one or several spots growing out of the uniform phase [Fig. 1(a) and Video 1 in [29]]. We observed that the lag time preceding pattern formation can range from a few to thousands α^{-1} and generically decreases with Γ and r (time scales are discussed more below and quantified in [29]). These spots have a spiral-like orientation of the actin fibers [Fig. 1(a), inset]. Remarkably, they are not stable but decay (after $\sim 200\ \alpha^{-1}$ for the present simulation) back to the uniform state. If fibers align faster than new ones are polymerized ($\Gamma = 4.3$), we again observe transient spot formation. Intriguingly, however, here we do not end up with a uniform phase but observe the emergence of traveling actin waves. These waves self-organize into a pattern with a well-defined length scale [Fig. 1(b) and Video 2 in [29]]. Further enhancing the alignment rate ($\Gamma = 10$) again leads to the formation of spots. Here, however, the spots are less pronounced and start to spiral and move while growing [26]; they continuously transform into traveling waves [Fig. 1(c) and Video 3 in [29]]. Further enhancing Γ directly leads to waves without a preceding spot stage. Therefore, strikingly, our simple and generic model accounts for the sequence of actin patterns, from spots to waves, observed experimentally [5,6]. We now want to understand why spots and then waves emerge.

Therefore, we perform a linear stability analysis of our equations of motion (providing results here in physical units). The present system has three uniform solutions. These are (i) $(\rho, \mathbf{p}) = (0, \mathbf{0})$ (which we chose as our initial state, following *in vivo* experiments), (ii) $(\rho, \mathbf{p}) = (\rho_0, \mathbf{0})$, and (iii) $(\rho, \mathbf{p}) = [\rho_0, \sqrt{(\gamma/\gamma_2)(\rho_0/\rho_c - 1)}\mathbf{e}]$, where $\mathbf{e}$ represents a unit vector pointing along a spontaneously chosen direction set by the initial conditions. All solutions correspond to uniform phases; the first two are unpolarized, the third is polarized and, hence, traveling (flocking). First, we explore the stability of our initial low-density state. The dominant branch of the dispersion relation for fluctuations around this phase reads $\lambda = \alpha - D_\rho \mathbf{q}^2$; therefore, our initial state is generally unstable against polymerization, simply leading to a density growth in the whole system if $\alpha > 0$ (with no effect on the polarization field, as the eigenmode of the unstable mode is orthogonal to $\mathbf{p}$). This density growth proceeds until we have $\rho = \rho_c$; i.e., polymerization generally transfers the system from phase (i) to phase (ii).

Conversely to phase (i), for $\rho_0 > \rho_c$, alignment interactions become effective in phase (ii) and dominate over rotational diffusion [Eq. (2)]. This can be seen from the dominant branch of the dispersion relation, $\lambda = \gamma(\rho_0/\rho_c - 1) - K\mathbf{q}^2$ (see [29]), for fluctuations in this phase, which yields a stationary long wavelength instability. Here, alignment interactions are strong enough to generate an instability of the uniform unpolarized phase but too weak to generate waves (which would require an oscillatory instability). Following this instability, the dynamical pathway of our system is subtle and can be described as follows. Actin fibers align locally, leading to polarized domains, with the polarization field of each domain pointing along a spontaneously chosen direction. Because of treadmilling, each of these domains moves but soon "collides" with others, resulting in a defect in the $\mathbf{p}$ field with ingoing F-actin flux from all directions (see Fig. 2), which in turn generates a spot in the density field [Figs. 1(a) and 1(b)]. This scenario is a natural and generic consequence of the instability of phase (ii) and therefore part of the dynamic pathway followed by our system, when initialized in phase (i). We determined the length scale of the spots, l, by a combination of linear stability analysis and systematic parameter sweeps (see [29]) and found that $l \sim \sqrt{K/[\gamma(\rho_0/\rho_c - 1)]}(\gamma_2 D_\rho/v_0^2)^{1/4}$. Hence, the typical spot size increases with diffusion but decreases with v_0. This scaling is intuitive, since fibers treadmill from all directions towards the spot center, thereby competing with diffusion (a similar scaling, albeit leading to a distinct functional form for l, determined the size of asters in Ref. [22]). Remarkably, we found that for $\gamma_2 D_\rho/v_0^2 > 1$ the spot size converges to a healing length $l \sim \sqrt{K/[\gamma(\rho_0/\rho_c - 1)]}$ representing the distance needed for the polarization field to recover from a local orientational perturbation (defect). We note that, in the absence of polymerization ($\alpha = 0$), our asters satisfy the steady state condition of Eq. (1) ($\dot{\rho} = 0$) yielding a solution $\mathbf{p} \propto \nabla\rho/\rho$, where fibers treadmill up the density gradient, thereby permanently balancing diffusive fiber losses. Importantly, however, the local density in the spot exceeds ρ_0, leading for $\alpha > 0$ to depolymerization. This initiates "Fisher waves" [25] traveling from the spot in all directions. We expect these Fisher wave fronts to move with a characteristic velocity of $v = \sqrt{2D_\rho\alpha}$; such waves combine with the alignment interactions to decrease spot size and take the system back towards a uniform phase. This scenario describes the transition from a uniform phase to spot formation and back to uniformity as observed in Fig. 1(a). But why does the described scenario not repeat to initiate new spots? The answer is that the new uniform phase is now polarized and given by (iii) rather than by (ii). Hence, the spots in Fig. 1(a) (Video 1 in [29]) are a generic

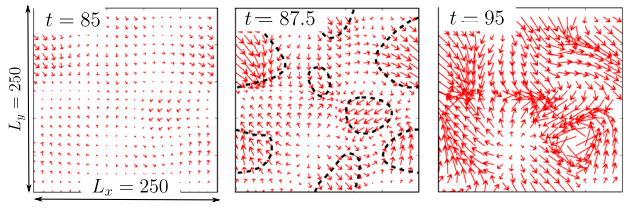

FIG. 2. Snapshots of the evolution of the $\mathbf{P}$ field during the formation of spots for $\Gamma = 4.3$, $r = 1.1$, $\mathcal{D} = 5$, and $\Gamma_2 = 0.075$, shown in Fig. 1(b).

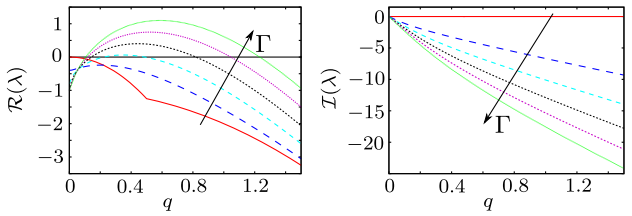

FIG. 3. Real and imaginary parts of the dispersion relation of the uniform polarized phase (iii), for $\Gamma = 0,\ 2,\ 4,\ 6,\ 8,\ 10$ (following the sense of the arrows), and with $r = 1.1$, $\mathcal{D} = 5$, and $\Gamma_2 = 0.075$.

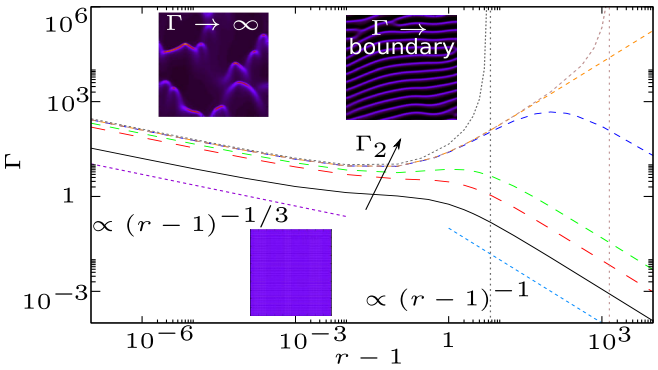

FIG. 4. Phase diagram with curves resulting from the linear stability analysis. They are consistent with numerical simulations (see [29]) and correspond to $\mathcal{D} = 5$ and Γ_2 equals 0.00075, 0.075, 0.1775, 0.3704, 3/8, 0.3754, and 0.4688 from bottom to top.

transient pattern formed as actin fibers polymerize starting from a low-density phase.

Having followed this pathway from phase (i) to phase (iii), we now want to understand how waves emerge. We therefore explore the stability of phase (iii) by calculating the dispersion relation for fluctuations around this phase (Fig. 3; see also [29]). Remarkably, $\mathcal{R}(\lambda)$ is always negative at small q but becomes positive at finite q if Γ is sufficiently large (Fig. 3). Since also the imaginary part of the dispersion relation is finite, we have an *oscillatory short wavelength* instability; hence, we may expect traveling waves for a sufficiently strong alignment (Γ): This explains our previous observation of traveling waves in Figs. 1(b) and 1(c). The velocity of our waves is given by $v \sim v_0\sqrt{(\gamma/\gamma_2)(\rho_0/\rho_c - 1)} = v_0 P_0$ if $r = (\rho_0/\rho_c - 1) > 1$ and $v \sim v_0\sqrt{\gamma/\gamma_2}$ otherwise. Therefore, the wave speed is proportional to the treadmilling velocity of individual fibers, weighted by an alignment factor, measuring the average fraction of aligned filaments. The distance between adjacent wave peaks can be estimated by a numerical evaluation of our dispersion relation, revealing a fastest-growing mode at length scale $l \propto l_1^{3/2} l_2^{-1/2}$ with $l_1 \sim \sqrt{K/\gamma}$ and $l_2 \sim \sqrt{KD_\rho/(v_0^2 P_0^2)}$ if $K > D_\rho$ or $l_2 \sim \sqrt{K^3/(D_\rho v_0^2 P_0^2)}$ if $K < D_\rho$ (see [29]; note we have dropped for simplicity an extra nondimensional dependence on r). Our simulations confirm that the wave separation is typically close to this value, at least deep into the wave-forming regime. We illustrate this by an explicit comparison of the linear stability analysis and simulations for all parameters in [29], showing that the above scaling predicts the correct trend but also that individual realizations show significant fluctuations. The width of our wave peaks follows, approximately, a variant of our healing length $l \sim \sqrt{K/\gamma}$ for $K > D_\rho$ and $l \sim \sqrt{D_\rho/\gamma}$ if $D_\rho > K$ (see [29])—in this context, this is the length scale over which diffusion neutralizes polar ordering within a wave peak.

It is also important to quantify typical time scales in the pattern formation cascade we observe. A characteristic time can be extracted from the inverse of the largest growth rate $1/\lambda_{\max}$ which scales as $1/[\gamma(r-1)^{1/3}]$ if $r - 1 < 1$ or $1/[\gamma(r-1)]$ if $r - 1 > 1$ (see [29]). This is an estimate for the time needed for the waves to emerge from the uniform polarized state (iii); hence, this is also the time scale over which we can observe transient spot formation.

The possible scenarios are summarized in a phase diagram (Fig. 4) which was constructed from a large set of simulations (see [29]). For small Γ and $r - 1$, i.e., when alignment interactions are weak and ρ_0 is close to the Onsager threshold, the evolution features a uniform increase of our low-density initial state, i.e., a transition from phase (i) via (ii); this phase then morphs into a set of asters and spirals, which leave way eventually to phase (iii), which is asymptotically stable. Instead, when we cross the transition line, we always find traveling actin waves at long time scales. Deep in the wave phase (large Γ), we find waves emerging directly from the uniform phase: these waves are normally irregular. Closer to the transition line, we instead find that spots appear before waves emerge; waves are here more regular, and the separation between peaks can be decreased by increasing polymerization (hence decreasing Γ). The different dynamics occur since, close to the transition line, waves emerge slowly, leaving enough time for spot formation. The length scale tunability may be linked to the fact that the longest wavelength in the instability band (where the real part of the dispersion relation is positive) depends on α. For $\Gamma_2 > 3/8$ (orange curve), there is an additional transition line in our phase diagram (dashed lines for gray and brown line), representing a parameter domain of large actin fiber density where waves are impossible even for very strong Γ. Physically, this means that wave formation is possible in our system only if self-propulsion is fast enough; the critical speed is given by a combination of fiber diffusion and alignment saturation.

In conclusion, we have shown that an ensemble of polymerizing and treadmilling actin filaments forms a cascade of patterns encompassing spots, spirals, and waves, which resemble the typical phenomenology found in

experiments. Specifically, when *Dictyostelium* cells recover from actin depolymerization, they reassemble their actin cytoskeleton by creating spots which later on transition to waves [6,13]. Remarkably, and at variance with previous work, our model recreates this sequence of patterns without the need to assume any underlying nonlinear biochemistry leading to delay, oscillatory, or activator-inhibitor behavior. Instead, starting from a low-density initial phase, we suggest that polymerization increases the overall density of actin until locally oriented actin flocks appear. These domains travel along randomly selected directions and collide with each other to form spirals or larger spots where the filament directions are arranged in an aster fashion. Hence, our work demonstrates that spots occur automatically en route from the typical low-density initial phase towards the flocking state featuring waves, thereby challenging previous and more complicated mechanisms describing the phenomenology of typical *in vivo* actin-wave experiments. Our results might also be useful to design and understand minimal *in vitro* systems mimicking the actin dynamics observed *in vivo*. Here, more complex patterns could be designed, e.g., by adding contractile myosin motors, which may lead to additional clustering instabilities of the uniform phase [22].

We thank Engineering and Physical Sciences Research Council (Grant No. EP/J007404/1) for support. B. L. gratefully acknowledges funding by a Marie Skłodowska Curie Intra European Fellowship (G. A. No. 654908) within Horizon 2020. We thank A. B. Goryachev for useful discussions.

*Corresponding author.
thomas.le-goff@ed.ac.uk
†Corresponding author.
bliebche@staffmail.ed.ac.uk

[1] B. Alberts, A. Johnson, J. Lewis, M. Raff, K. K. Roberts, and P. Walter, *Molecular Biology of the Cell* (Garland Science, New York, 2002).
[2] D. Bray, *Cell Movements* (Garland Science, New York, 2000).
[3] A. Gholami, M. Falcke, and E. Frey, New J. Phys. **10**, 033022 (2008).
[4] V. Schaller, C. Weber, C. Semmrich, E. Frey, and A. R. Bausch, Nature (London) **467**, 73 (2010); J. F. Joanny and S. Ramaswamy, Nature (London) **467**, 33 (2010).
[5] G. Gerisch, T. Bretschneider, A. Müller-Taubenberger, E. Simmeth, M. Ecke, S. Diez, and K. Anderson, Biophys. J. **87**, 3493 (2004).
[6] T. Bretschneider, K. Anderson, M. Ecke, A. M. Müller-Taubenberger, B. Schroth-Diez, H. C. Ishikawa-Ankerhold, and G. Gerisch, Biophys. J. **96**, 2888 (2009).
[7] J. Allard and A. Mogilner, Curr. Opin. Cell Biol. **25**, 107 (2013).
[8] M. G. Vicker, Biophys. Chem. **84**, 87 (2000).
[9] M. G. Vicker, Exp. Cell Res. **275**, 54 (2002).
[10] V. Kamviwath, J. Hu, and H. G. Othmer, PLoS One **8**, e64272 (2013).
[11] A. Y. Pollitt and R. H. Insall, J. Cell Sci. **122**, 2575 (2009).
[12] O. D. Weiner, W. A. Marganski, L. F. Wu, S. J. Altschuler, and M. W. Kirschner, PLoS Biol. **5**, e221 (2007).
[13] S. Whitelam, T. Bretschneider, and N. J. Burroughs, Phys. Rev. Lett. **102**, 198103 (2009).
[14] V. Wasnik and R. Mukhopadhyay, Phys. Rev. E **90**, 052707 (2014).
[15] A. E. Carlsson, Phys. Rev. Lett. **104**, 228102 (2010).
[16] K. Doubrovinski and K. Kruse, Europhys. Lett. **83**, 18003 (2008).
[17] C. Beta, PMC Biophys. **3**, 12 (2010).
[18] J. Toner, Phys. Rev. Lett. **108**, 088102 (2012).
[19] L. Onsager, Ann. N.Y. Acad. Sci. **51**, 627 (1949).
[20] Considering a reaction $\alpha - \beta\rho$, with α, $\beta > 0$, leads to similar results; this is less justified biophysically, as it requires *de novo* F-actin nucleation (infrequent in practice).
[21] S. Mishra, A. Baskaran, and M. C. Marchetti, Phys. Rev. E **81**, 061916 (2010).
[22] A. Chaudhuri, B. Bhattacharya, K. Gowrishankar, S. Mayor, and M. Rao, Proc. Natl. Acad. Sci. U.S.A. **108**, 14825 (2011); K. Gowrishankar and M. Rao, Soft Matter **12**, 2040 (2016).
[23] J. Toner, Y.-h. Tu, and S. Ramaswamy, Ann. Phys. (Amsterdam) **318**, 170 (2005).
[24] J.-B. Caussin, A. Solon, A. Peshkov, H. Chaté, T. Dauxois, J. Tailleur, V. Vitelli, and D. Bartolo, Phys. Rev. Lett. **112**, 148102 (2014).
[25] W. van Saarloos, Phys. Rep. **386**, 29 (2003).
[26] X. Yang, D. Marenduzzo, and M. C. Marchetti, Phys. Rev. E **89**, 012711 (2014).
[27] M. Bailly, F. Macaluso, M. Cammer, A. Chan, J. E. Segall, and J. S. Condeelis, J. Cell Biol. **145**, 331 (1999).
[28] F. D. C. Farrell, M. C. Marchetti, D. Marenduzzo, and J. Tailleur, Phys. Rev. Lett. **108**, 248101 (2012).
[29] See Supplemental Material at http://link.aps.org/supplemental/10.1103/PhysRevLett.117.238002 for details on the linear stability analysis, a quantitative discussion of time scales and length scales, and additional simulation results.